

1 **Model Comparisons Between Canonical Vine Copulas and Meta-Gaussian**  
2 **for Forecasting Agricultural Drought over China**

3 Authors: Haijiang Wu<sup>1,2</sup>, Xiaoling Su<sup>1,2\*</sup>, Vijay P. Singh<sup>3,4</sup>, Te Zhang<sup>2</sup>, Jixia Qi<sup>2</sup>, and

4 Shengzhi Huang<sup>5</sup>

5 Affiliation:

6 <sup>1</sup>*Key Laboratory for Agricultural Soil and Water Engineering in Arid Area of Ministry of Education,*  
7 *Northwest A&F University, Yangling, Shaanxi, 712100, China*

8 <sup>2</sup>*College of Water Resources and Architectural Engineering, Northwest A&F University, Yangling,*  
9 *Shaanxi, 712100, China*

10 <sup>3</sup>*Department of Biological and Agricultural Engineering & Zachry Department of Civil and*  
11 *Environmental Engineering, Texas A&M University, College Station, TX 77843-2117, USA*

12 <sup>4</sup>*National Water and Energy Center, UAE University, Al Ain, UAE*

13 <sup>5</sup>*State Key Laboratory Base of Eco-Hydraulic Engineering in Arid Area, Xi'an University of*  
14 *Technology, Xi'an, Shaanxi, 710048, China*

15 \*Corresponding Author:

16 Dr. Xiaoling Su, College of Water Resources and Architectural Engineering, Northwest A&F  
17 University, Weihui Road 23, Yangling, Shaanxi, China, *Email: [xiaolingsu@nwafu.edu.cn](mailto:xiaolingsu@nwafu.edu.cn)* (X. Su).

18

19

20

## 21 **Abstract**

22       Agricultural drought is mainly caused by reduced soil moisture and precipitation and shows  
23 adverse impacts on the growth of crops and vegetation, thus affecting agricultural production and  
24 food security. For developing measures for drought mitigation, reliable agricultural drought  
25 forecasting is essential. In this study, we developed an agricultural drought forecasting model based  
26 on canonical vine copulas under three-dimensions (3C-vine model), in which the antecedent  
27 meteorological drought and agricultural drought persistence were utilized as predictors. Besides, the  
28 meta-Gaussian (MG) model was selected as a reference model to evaluate the forecast skill. The  
29 agricultural drought in August of 2018 was selected as a typical case study, and the spatial patterns  
30 of 1–3-month lead forecasts of agricultural drought utilizing the 3C-vine model resembled the  
31 corresponding observations, indicating the good predictive ability of the model. The performance  
32 metrics (NSE,  $R^2$ , and RMSE) showed that the 3C-vine model outperformed the MG model for  
33 forecasting agricultural drought in August under diverse lead times. Also, the 3C-vine model  
34 exhibited excellent forecast skills in capturing the extreme agricultural drought over different  
35 selected typical regions. This study may help to guide drought early warning, drought mitigation,  
36 and water resources scheduling.

37 **Keywords:** drought forecasting, model comparison, vine copulas, meta-Gaussian

## 38 **1. Introduction**

39       Agriculture is the source of livelihoods of over 2.5 billion people worldwide, and the  
40 agricultural sector also sustains 82% of all drought impacts (FAO, 2021). A cascade of impacts of  
41 droughts, such as crop reduction and failure, increased human and tree mortality, and ecological  
42 disturbance, have attracted considerable attention (FAO, 2021; Lu et al., 2012; Modanesi et al., 2020;

43 Su et al., 2018; Zhang et al., 2018; Zhang et al., 2019; Zscheischler et al., 2020). Droughts have  
44 reduced global crop production by about 9–10% for the period 1964–2007 (Lesk et al., 2016).  
45 Additionally, droughts have caused overall crop and livestock production loss of \$37 billion over  
46 the least developed and lower-middle-income countries (FAO, 2021). Agricultural drought  
47 forecasting, therefore, lies at the core of overall drought risk management and is critical for food  
48 security, early warning, as well as drought preparedness and mitigation.

49 Agricultural drought is generally referred to as soil moisture shortage, which adversely affects  
50 crop yield and vegetation health (Modanesi et al., 2020; Zhang et al., 2016; Zhang et al., 2021).  
51 Under natural conditions, atmospheric precipitation is a paramount source for replenishment of soil  
52 moisture (Wu et al., 2021a). Therefore, reduced soil moisture (agricultural drought) mainly arises  
53 from precipitation deficit (meteorological drought) (Modanesi et al., 2020; Orth and Destouni, 2018).  
54 Moreover, soil moisture has a good memory to drought because of the time-integration effects (Long  
55 et al., 2019), i.e., agricultural drought persistence. Previous meteorological drought and antecedent  
56 agricultural drought can be taken into consideration as predictors of subsequent agricultural drought.

57 In hydrology, some physically-based hydrological models (e.g., Distributed Time-Variant Gain  
58 Hydrological Model (DTVGM; Ma et al, 2021) and Soil and Water Assessment Tool (SWAT; Wu et  
59 al., 2019)) are widely used in hydrological simulation and prediction, the droughts included as well.  
60 However, the physically-based hydrological models typically apply to a catchment or sub-regional  
61 scale, and generally require numerous hydrometeorological variables to achieve more accurate real-  
62 time predictions (Liu et al., 2021a; Xu et al., 2021a). Traditional methods, such as regression models,  
63 machine learning models, and hybrid models (by considering both statistical and dynamical  
64 predictions) (Hao et al., 2016), have been extensively employed to forecast drought. Yet, these

65 models tend to be limited in considering the complex nonlinear (e.g., regression models), explicit  
66 physical mechanisms and over-fitting (e.g., machine learning models), as well as the demand of  
67 massive hydroclimatic data input (e.g., hybrid models). The copula functions, first introduced by  
68 Sklar (1959), overcome the limitations of the abovementioned conventional statistical methods; and  
69 the applications of copulas in hydrology and geosciences go back to the 2000s (e.g., De Michele and  
70 Salvadori, 2003; Favre et al., 2004; Salvadori and De Michele, 2004). Since copulas are flexible  
71 joining arbitrary marginal distributions of variables, they have been widely employed in  
72 hydrological research community, such as frequency analysis and risk assessment (De Michele et  
73 al., 2013; Hao et al., 2017; Liu et al., 2021b; Sarhadi et al., 2016; Xu et al., 2021b; Zhang et al.,  
74 2021; Zhou et al., 2019), flood and runoff forecasting (Bevacqua et al., 2017b; Hemri et al., 2015;  
75 Liu et al., 2018; Zhang and Singh, 2019), and drought forecasting (Ganguli and Reddy, 2014; Wu et  
76 al., 2021a). However, when bivariate copulas are extended to higher-dimensional ( $\geq$  three-  
77 dimensions) cases, they are restricted due to nonexistence of analytical expressions (Liu et al.,  
78 2021a). Symmetric Archimedean copulas and nested Archimedean copulas partially have addressed  
79 the issues of dimensionality, but single parameter and Archimedean class are difficult to characterize  
80 the various dependence structures (Aas and Berg, 2009; Hao et al., 2016; Wu et al., 2021a).  
81 Fortunately, the vine copulas, which have been developed by Joe (1996) as well as Bedford and  
82 Cooke (2002), can be adopted to address these limitations.

83 Vine copulas are flexible in decomposing any multi-dimensional joint distribution into a  
84 hierarchy of bivariate copulas or pair copula constructions (Aas et al., 2009; Bedford and Cooke,  
85 2002; Liu et al., 2021a; Vernieuwe et al., 2015; Xiong et al., 2014). These copulas have been  
86 extensively applied in the hydrological field (Bevacqua et al., 2017b; Liu et al., 2021b; Vernieuwe

87 et al., 2015; Wu et al., 2021a). For instance, Xiong et al. (2014) derived the annual runoff  
88 distributions using canonical vine copulas. Liu et al. (2018) developed a framework to investigate  
89 compound floods based on canonical vine copulas. Wang et al. (2019) utilized regular vine copulas  
90 with historical streamflow and climate drivers to simulate monthly streamflow for the headwater  
91 catchment of the Yellow River basin. Liu et al. (2021a) developed a hybrid ensemble forecast model,  
92 using the Bayesian model averaging combined canonical vine copulas, to forecast water level. Wu  
93 et al. (2021a) proposed an agricultural drought forecast model based on vine copulas under four-  
94 dimensional scenarios.

95 The meta-Gaussian (MG) model, a popular statistical model in the hydrometeorological  
96 community, has explicit conditional distributions, which is apt for forecasting and risk assessment  
97 purposes (Hao et al., 2016; Hao et al., 2019a; Wu et al., 2021b; Zhang et al., 2021). The forecast  
98 skills of the MG model for drought or compound dry-hot events, for example, outperformed the  
99 persistence-based or random forecast models (Hao et al., 2016; Hao et al., 2019a; Wu et al., 2021b).  
100 However, the MG model only depicts the linear relationship among explanatory variables (predictors)  
101 and forecasted variable via covariate matrix, it cannot characterize the nonlinear or tail dependence  
102 existing in the variables (Hao et al., 2016). Fortunately, Vine copulas can flexibly combine multiple  
103 variables via bivariate copula to characterize numerous or complex dependencies. There has been a  
104 rather limited investigation, to our knowledge, that conducting model comparisons between vine  
105 copulas and MG for agricultural drought forecasting under the same conditions. Therefore,  
106 investigations on drought forecasting skills between vine copulas and the MG model are needed to  
107 obtain more reliable drought forecasts.

108 The objective of this study therefore was to compare the forecast ability of agricultural drought

109 in August of every year in the period 1961–2018 between canonical vine copulas (i.e., 3C-vine  
110 model) and MG model under three-dimensional scenario. In the following, we briefly describe the  
111 study area and data used in Section 2. The MG and 3C-vine models and performance metrics utilized  
112 are presented in Section 3. Results of the 3C-vine model application and assessment are displayed  
113 in Section 4. Finally, the discussion and conclusions are presented in Section 5.

## 114 **2. Study area and data used**

115 China stretches across a vast area covering diverse climate regimes and is a major agricultural-  
116 producing country (Wu et al., 2021a; Zhang et al., 2015). For the convenience of analyzing spatial  
117 patterns of agricultural drought, the climate of China was divided into seven sub-climate regions on  
118 the basis of Zhao (1983) and Yao et al. (2018), as shown in Figure 1. For each sub-climate region,  
119 the temperature and moisture conditions when combined are roughly similar, and the type of soil  
120 and vegetation have a certain common characteristic (Zhao, 1983).

121 -----**Figure 1.**-----

122 In this study, the gridded monthly precipitation with a  $0.25^{\circ} \times 0.25^{\circ}$  spatial resolution was  
123 obtained from the CN05.1 dataset for the 1961–2018 period over the mainland of China (excluding  
124 the Taiwan province), which was provided by the Climate Change Research Center, Chinese  
125 Academy of Sciences (available at <http://ccrc.iap.ac.cn/resource/detail?id=228>). The Copernicus  
126 Climate Change Service (C3S) at European Center for Medium-Range Weather Forecast (ECMWF)  
127 has begun the release of the ERA5 back extension data covering the period 1950–1978 on the  
128 Climate Data Store (CDS). Therefore, the gridded monthly soil moisture with a  $0.25^{\circ} \times 0.25^{\circ}$  spatial  
129 resolution corresponding to three soil depths (0–7 cm, 7–28 cm, and 28–100 cm) are available from  
130 the ECMWF ERA5 reanalysis datasets for 1961–1978:

131 [https://cds.climate.copernicus.eu/cdsapp#!/dataset/reanalysis-era5-single-levels-monthly-means-](https://cds.climate.copernicus.eu/cdsapp#!/dataset/reanalysis-era5-single-levels-monthly-means-preliminary-back-extension?tab=overview)  
132 [preliminary-back-extension?tab=overview](https://cds.climate.copernicus.eu/cdsapp#!/dataset/reanalysis-era5-single-levels-monthly-means?tab=overview) and 1979–2018:  
133 [https://cds.climate.copernicus.eu/cdsapp#!/dataset/reanalysis-era5-single-levels-monthly-](https://cds.climate.copernicus.eu/cdsapp#!/dataset/reanalysis-era5-single-levels-monthly-means?tab=overview)  
134 [means?tab=overview](https://cds.climate.copernicus.eu/cdsapp#!/dataset/reanalysis-era5-single-levels-monthly-means?tab=overview). The CN05.1 and ERA5 reanalysis datasets have been extensively utilized  
135 numerous studies, e.g., drought monitoring and forecasting (Wu et al., 2021a; Zhang et al., 2021),  
136 long-term climatic analysis (He et al., 2021; Wu et al., 2017), and flash drought attribution analysis  
137 (Wang and Yuan, 2021).

### 138 3. Methodology

139 The Standardized Precipitation Index (SPI, based on monthly precipitation) and Standardized  
140 Soil moisture Index (SSI, based on monthly cumulative soil moisture at top-three soil depths) is  
141 leveraged to characterize meteorological drought and agricultural drought at a 6-month timescale,  
142 respectively. The empirical Gringorten plotting position formula (Gringorten, 1963) was used to  
143 obtain the empirical cumulative probabilities of these two indexes, which were then transformed  
144 into standardized variables via the normal quantile transformation. Since meteorological drought is  
145 a source of other drought types (e.g., agricultural drought), the antecedent precipitation deficiency  
146 (i.e., meteorological drought) has a stronger effect on the subsequent soil moisture deficiency (i.e.,  
147 agricultural drought). Moreover, soil moisture has a good memory for prior drought, i.e., agricultural  
148 drought persistence, which is attributed to the soil porosity characteristics and time-integration  
149 effects (Long et al., 2019; Wu et al., 2021a).

150 We attempted to use the prior meteorological drought ( $SPI_{t-i}$ ;  $t$  denotes the target month (e.g.,  
151 August), and  $i$  indicates lead time (month)) and agricultural drought persistence ( $SSI_{t-i}$ ) to forecast  
152 the subsequent agricultural drought ( $SSI_t$ ) based on the canonical vine copulas under three-

153 dimensional scenarios (3C-vine model). We selected the meta-Gaussian (MG) model as a reference  
 154 model to assess the agricultural drought forecast performance of the 3C-vine model. Here, the 6-  
 155 month timescale SPI (SSI) in August, which is calculated by the cumulative precipitation (soil  
 156 moisture) from March to August, can indirectly reflect the surplus or deficit situations of water in  
 157 spring (March-April-May) and summer (June-July-August) seasons. Furthermore, August is a key  
 158 growth period for crops (e.g., anthesis, fruiting, and seed filling) and vegetation and is also a period  
 159 with frequent droughts (Wu et al., 2021a). Undoubtedly, agricultural drought forecast can be  
 160 implemented in any month of interest, based on 3C-vine model and MG model. More detailed  
 161 information is given below.

### 162 **3.1. Meta-Gaussian model under three-dimensional scenarios**

163 Meta-Gaussian (MG) model can effectively combine multiple hydrometeorological variables,  
 164 which have gained attention for drought forecasting and risk assessment (Hao et al., 2019a; Hao et  
 165 al., 2019b; Wu et al., 2021b; Zhang et al., 2021). Suppose the series of  $SPI_{t-i}$ ,  $SSI_{t-i}$ , and  $SSI_t$   
 166 correspond to random variables  $Y_1$ ,  $Y_2$ , and  $Y_3$ , respectively, the predictand  $y_3$  under the given  
 167 conditions of  $y_1$  and  $y_2$  based on the MG model can be expressed as (Wilks, 2014):

$$168 \quad y_3 | (y_1, y_2) \sim N(\mu_{y_3|(y_1, y_2)}, \Sigma_{y_3|(y_1, y_2)}) \quad (1)$$

169 where  $N$  signifies the Gaussian distribution function;  $\mu_{y_3|(y_1, y_2)}$  denotes the conditional mean; and  
 170  $\Sigma_{y_3|(y_1, y_2)}$  represents the conditional covariate matrix.

171 Furthermore, we removed the forecast values in a specific year of  $y_1$ ,  $y_2$ , and  $y_3$ , which denote  
 172  $y_1^{-yr}$ ,  $y_2^{-yr}$ , and  $y_3^{-yr}$ , respectively. Under this circumstance, the covariate matrix  $\Sigma$  regarding  $y_1^{-yr}$ ,  
 173  $y_2^{-yr}$ , and  $y_3^{-yr}$  can be written as:



$$174 \quad \mathbf{\Sigma} = Cov \begin{bmatrix} (y_1^{-yr}, y_1^{-yr}) & (y_1^{-yr}, y_2^{-yr}) & (y_1^{-yr}, y_3^{-yr}) \\ (y_2^{-yr}, y_1^{-yr}) & (y_2^{-yr}, y_2^{-yr}) & (y_2^{-yr}, y_3^{-yr}) \\ (y_3^{-yr}, y_1^{-yr}) & (y_3^{-yr}, y_2^{-yr}) & (y_3^{-yr}, y_3^{-yr}) \end{bmatrix} = \begin{bmatrix} Cov_{11} & Cov_{12} & Cov_{13} \\ Cov_{21} & Cov_{22} & Cov_{23} \\ Cov_{31} & Cov_{32} & Cov_{33} \end{bmatrix} = \begin{bmatrix} \mathbf{\Sigma}_{11} & \mathbf{\Sigma}_{12} \\ \mathbf{\Sigma}_{21} & \mathbf{\Sigma}_{22} \end{bmatrix} \quad (2)$$

175 where  $Cov_{mn} = Cov(y_m^{-yr}, y_n^{-yr})$  denotes the covariance between  $y_m^{-yr}$  and  $y_n^{-yr}$  ( $m = 1, 2, 3; n = 1,$   
176  $2, 3$ ). The forecast of specific years, i.e.,  $y_3^{yr}$ , can be derived as (Wilks, 2014):

$$177 \quad y_3^{yr} = \mu_{y_3^{-yr}} + \mathbf{\Sigma}_{21} \mathbf{\Sigma}_{11}^{-1} \begin{bmatrix} y_1^{yr} - \mu_{y_1^{-yr}} \\ y_2^{yr} - \mu_{y_2^{-yr}} \end{bmatrix} \quad (3)$$

178 where  $\mu_{y_1^{-yr}}$ ,  $\mu_{y_2^{-yr}}$ , and  $\mu_{y_3^{-yr}}$  represent the mean of  $y_1^{-yr}$ ,  $y_2^{-yr}$ , and  $y_3^{-yr}$ , respectively;  $y_1^{yr}$  and  
179  $y_2^{yr}$  denote that  $y_1$  and  $y_2$  provided the forecast information at time  $t-i$  in a specific year. More details  
180 about forecasting agricultural drought based on the MG model can be found in Figure 3.

### 181 **3.2. Canonical vine copulas model under three-dimensional scenarios**

182 Copulas can effectively combine multiple variables without the restriction of marginal  
183 distributions (Nelsen, 2013; Sarhadi et al., 2016; Wang et al., 2019; Xiong et al., 2014). They were  
184 initially utilized for deriving joint distributions of two-dimensional variables, since parameters are  
185 easy to assess and the analytical solution is apt to obtain (Liu et al., 2021a; Sadegh et al., 2017).  
186 However, under higher-dimensional (e.g.,  $d \geq 3$ ) scenarios, owing to the limitations of a great deal  
187 of parameters and complexity, the copulas (mainly referred to bivariate copulas) are difficult to  
188 promote and apply (Joe, 2014; Liu et al., 2018; Liu et al., 2021a; Sadegh et al., 2017). To overcome  
189 these limitations, Joe (1996) and Aas et al. (2009) developed vine copulas, a hierarchy of pair copula  
190 constructions, for multi-dimensional cases. Vine copulas possess two sub-classes: canonical vine  
191 copulas (C-vine copulas) and drawable vine copulas (D-vine copulas). Here, we mainly employed  
192 the C-vine copulas to establish the forecast model of agricultural drought under three-dimensional

193 conditions. Undoubtedly, a similar scheme is capable of applying to D-vine copulas.

194 C-vine copulas may have numerous tree structures, especially for the case of higher dimensions,  
195 which are associated with the quantity and ordering of variables (Aas et al., 2009; Liu et al., 2018;  
196 Liu et al., 2021a; Wu et al., 2021a). Also, different ordering of variables affects the estimation of the  
197 parameters of C-vine copulas (Liu et al., 2021a; Wang et al., 2019). Given the ordering of variables  
198  $Y_1$ ,  $Y_2$ , and  $Y_3$  for three-dimensional C-vine copula model (termed as 3C-vine model hereinafter;  
199 Figure 2a), the joint probability density function (PDF),  $g_{123}$ , can be expressed as (Aas et al., 2009):

$$200 \quad g_{123} = g_1 \cdot g_2 \cdot g_3 \cdot c_{12} \cdot c_{13} \cdot c_{23|1} \quad (4)$$

201 where  $g_1$ ,  $g_2$ , and  $g_3$  correspond to the margin density functions of  $g_1(y_1)$ ,  $g_2(y_2)$ , and  $g_3(y_3)$ ,  
202 respectively;  $c$  is the bivariate copula density;  $c_{12}$ ,  $c_{13}$ , and  $c_{23|1}$  signify the abbreviation of  $c_{1,2}[G_1(y_1)$ ,  
203  $G_2(y_2)]$ ,  $c_{1,3}[G_1(y_1)$ ,  $G_3(y_3)]$ , and  $c_{2,3|1}[G(y_2|y_1)$ ,  $G(y_3|y_1)]$ , respectively. The  $G_m(y_m)$  corresponds to  
204 cumulative density function (CDF) of the  $y_m$ ;  $G(y_2|y_1)$  denotes the conditional probability  
205 distribution of  $y_2$  under known conditions of  $y_1$ , that is similar for  $G(y_3|y_1)$ . The Gaussian (or Normal),  
206 Student-t, Clayton, and Frank copulas, as well as their rotated (survival) forms (Dißmann et al., 2013;  
207 Liu et al., 2021b) are utilized to obtain the optimal internal bivariate copulas for distinct trees in 3C-vine  
208 model based on the Akaike information criterion (AIC). With the help of *CDVineCondFit* R function in  
209 “*CDVineCopulaConditional*” R package (Bevacqua, 2017a), based on the AIC, we selected the optimal  
210 tree structures (i.e., detected the suitable variable ordering; seen in Figure 2).

211 -----**Figure 2.**-----

212 A conditional copula density needs to be addressed in Equation 4, i.e.,  $G(y|\mathbf{w})$ , where  $\mathbf{w}$  is a  $d$ -  
213 dimensional vector  $\mathbf{w} = (w_1, \dots, w_d)$ . Here, regarding the conditional distribution of  $y$  given the

214 conditions  $\mathbf{w}$ , we introduced the  $h$ -function,  $h(y, \mathbf{w}; \theta)$ , to indicate the  $G(y|\mathbf{w})$  as follows (Aas et al.,  
 215 2009; Joe, 1996):

$$216 \quad h(y, \mathbf{w}; \theta) := G(y | \mathbf{w}) = \frac{\partial C_{y, w_j | \mathbf{w}_{-j}} [G(y | \mathbf{w}_{-j}), G(w_j | \mathbf{w}_{-j})]}{\partial G(w_j | \mathbf{w}_{-j})} \quad (5)$$

217 where  $\theta$  denotes the parameter(s) of bivariate copula function  $C_{y, w_j | \mathbf{w}_{-j}}$ ;  $w_j$  represents an arbitrary  
 218 component of  $\mathbf{w}$ ; and  $\mathbf{w}_{-j}$  indicates the excluding element  $w_j$  from the vector  $\mathbf{w}$ .

219 Let the ordering variables be  $y_1, y_2$ , and  $y_3$ , the conditional variables be  $y_1$  and  $y_2$ , and the  
 220 predictand be  $y_3$ . Accordingly, the expression of  $G(y_3|y_1, y_2)$ , based on Equation 5, can be written as:

$$221 \quad G(y_3 | y_1, y_2) = \frac{\partial C_{y_3, y_1 | y_2} [G(y_3 | y_1), G(y_2 | y_1)]}{\partial G(y_2 | y_1)} = h \{ h(u_3 | u_1; \theta_{12}) | h(u_2 | u_1; \theta_{11}); \theta_{21} \} \quad (6)$$

222 where  $\theta_{ij}$  ( $i$  denotes a tree and  $j$  is an edge) represents the parameters of different conditional copulas  
 223 in the 3C-vine model (Figure 2a); and  $u_k$  ( $k = 1, 2, 3$ ) is the marginal CDF of  $y_k$ . The CDF for each  
 224 variable is substituted by the corresponding empirical Gringorten cumulative probability (Bevacqua  
 225 et al., 2017b; Genest et al., 2009; Wu et al., 2021a).

226 Here, we introduced the  $\tau$ -th copula–quantile curve (Chen et al., 2009; Liu et al., 2018) to  
 227 simulate  $u_3$  based on Equation 6 and derived its inverse distribution function as follows:

$$228 \quad y_3 = N^{-1} \{ G(\tau | y_1, y_2) \} = N^{-1}(u_3) = N^{-1} \left[ h^{-1} \left\{ h^{-1}(\tau | h(u_2 | u_1; \theta_{11}); \theta_{21}) | u_1; \theta_{12} \right\} \right] \quad (7)$$

229 where  $N^{-1}$  and  $h^{-1}$  signify the inverse form of Gaussian distribution and  $h$ -function, respectively;  $y_3$   
 230 is the forecasted agricultural drought at time  $t$  (i.e.,  $SSI_t$ );  $y_1$  and  $y_2$  are the predictors corresponding  
 231 to the antecedent meteorological drought and agricultural drought persistence at time  $t-i$  (i.e.,  $SPI_{t-i}$   
 232 and  $SSI_{t-i}$ ). The R functions of *BiCopHfunc* and *BiCopHinv* in the R package “*VineCopula*” (Nagler  
 233 et al., 2021) were utilized to model the  $h$ -function and its inverse form for Equation 7, respectively.

234 The tree structure is related to the ordering variables, so when the ordering variables are  $y_2, y_1,$   
 235 and  $y_3$  (conditional variables are  $y_1$  and  $y_2$ ; Figure 2b), Equations 6 and 7 can be changed analogously  
 236 as:

$$237 \quad G(y_3 | y_2, y_1) = h \left\{ h(u_3 | u_2; \theta_{12}) | h(u_1 | u_2; \theta_{11}); \theta_{21} \right\} \quad (8)$$

$$238 \quad y_3 = N^{-1}(u_3) = N^{-1} \left[ h^{-1} \left\{ h^{-1}(\tau | h(u_1 | u_2; \theta_{11}); \theta_{21}) | u_2; \theta_{12} \right\} \right] \quad (9)$$

239 With agricultural drought forecast via 3C-vine model, as the details presented in Figure 3, we  
 240 first selected the best 3C-vine model (i.e., selected the best model from Equations 7 and 9 according  
 241 to minimum AIC). Then, a sample size of 1,000 uniformly distributed random values was generated  
 242 over the interval  $[0, 1]$  by Monte Carlo simulation. Last, the best 3C-vine model was utilized to  
 243 obtain 1,000 simulations (or estimations) for  $y_3^{yr}$ . The best forecast of  $y_3^{yr}$  was finally calculated by  
 244 the mean value of these simulations. Note that the leave-one-out cross validation (LOOCV) (Wilks,  
 245 2014) is applied to forecast agricultural drought for each grid cell in August of every year during  
 246 1961–2018 based on the 3C-vine model or MG model, namely, each time one sample (or observation)  
 247 was left for validation, and the rest were used to establish 3C-vine model or MG model and obtain  
 248 the corresponding parameters of these models. In other words, this process was repeated 58 times  
 249 (the length of years used in this study) for a specific grid cell.

250 -----**Figure 3.**-----

### 251 **3.3. Performance metrics**

252 Three evaluation metrics: Nash-Sutcliffe efficiency (NSE), coefficient of determination ( $R^2$ ),  
 253 and root mean square error (RMSE), were utilized to assess the forecast performance of 3C-vine  
 254 model and MG model. These metrics can be expressed as:

$$255 \quad NSE = 1 - \frac{\sum_{i=1}^n (AP_i - AO_i)^2}{\sum_{i=1}^n (AO_i - \overline{AO})^2} \quad NSE \in (-\infty, 1] \quad (10)$$

$$256 \quad R^2 = \frac{\left[ \sum_{i=1}^n (AO_i - \overline{AO})(AP_i - \overline{AP}) \right]^2}{\sum_{i=1}^n (AO_i - \overline{AO})^2 \cdot \sum_{i=1}^n (AP_i - \overline{AP})^2} \quad R^2 \in [0, 1] \quad (11)$$

$$257 \quad RMSE = \sqrt{\frac{1}{n} \sum_{i=1}^n (AP_i - AO_i)^2} \quad RMSE \in [0, +\infty) \quad (12)$$

258 where  $n$  is the number of forecast periods;  $AO_i$  and  $AP_i$  are the  $i$ -th observed and forecasted  
 259 agricultural droughts (i.e., SSI), respectively;  $\overline{AO}$  and  $\overline{AP}$  denote the mean of the SSI  
 260 observations and forecasts in the target month (e.g., August), respectively. Moreover, a most positive  
 261  $NSE$  and  $R^2$  value and a lower  $RMSE$  value indicate a good forecast performance for the 3C-vine  
 262 model or MG model.

## 263 4. Results

### 264 4.1. Correlation patterns of agricultural drought with potential predictors

265 The dependence between variables can be measured by the correlation coefficient, indirectly  
 266 characterizing the quantity of common information between two variables. We employed Kendall's  
 267 correlation coefficient ( $\tau_k$ ) to measure the dependence of agricultural drought at current time  $t$  (SSI $_t$ ,  
 268 herein  $t$  is August) with the previous meteorological drought (SPI $_{t-i}$ ,  $i$  indicates the lag or lead times  
 269 with 1–3-month herein) and agricultural drought persistence (SSI $_{t-i}$ ). It should be mentioned that the  
 270 significant correlation prevalent used may overestimate or overinterpret the dependence between  
 271 variables (Wilks, 2016). Therefore, we adopted the maximum false discovery rate (FDR) of 0.1 to  
 272 correct  $\tau_k$  at the 0.05 significance level (Benjamini and Hochberg, 1995; Röthlisberger and Martius,

273 2019; Wilks, 2016).

274 -----**Figure 4.**-----

275 Figure 4 summarizes 1–3-month lag  $\tau_k$  between antecedent SPI (SSI) and succedent SSI for  
276 August during 1961–2018 over China. For most regions of China under 1–3-month lag times, the  
277 previous meteorological drought or agricultural drought persistence (memory) showed significant  
278 positive correlations (i.e., the stippling in Figure 4) with the target agricultural drought. Also, we  
279 found perfect agricultural drought memory over many regions of China (excluding D4, a humid  
280 climate region) (Figures 4e and 4f), as the overlapping information existed in  $SSI_t$  and  $SSI_{t-i}$ .  
281 Additionally, the dependency pattern varied temporally and spatially, and this phenomenon  
282 evidently occurred with the lag (or lead) time extended, especially between  $SPI_{t-i}$  and  $SSI_t$  (Figures  
283 4a–4c). Overall, the prior meteorological drought and agricultural drought memory provided reliable  
284 and useful forecast information for the subsequent agricultural drought for most areas of China.

#### 285 **4.2. Forecast performance comparison between 3C-vine model and MG Model**

286 We leveraged the MG model as a reference model to measure the performance of 3C-vine  
287 model in forecasting agricultural drought for the period 1961–2018 over China. Figures 5a–5i show  
288 the difference in  $NSE$ ,  $R^2$ , and  $RMSE$  between 3C-vine and MG models, i.e.,  $\Delta NSE = NSE_{3C} - NSE_{MG}$ ,  
289  $\Delta R^2 = R^2_{3C} - R^2_{MG}$ , and  $\Delta RMSE = RMSE_{3C} - RMSE_{MG}$  under 1–3-month lead times for August,  
290 respectively. In terms of the spatial extent of  $\Delta NSE > 0$ ,  $\Delta R^2 > 0$ , and  $\Delta RMSE < 0$ , the agricultural  
291 drought forecast ability of 3C-vine model superior MG model was occupied 65%, 68%, and 58% of  
292 land areas in China, respectively, under the 1-month lead SSI forecast (Figures 5a, 5d, and 5g). The  
293 relationship between predictors and the forecasted variable was simple under 1–month lead time, so  
294 the MG model better showed their connection. However, with the lead time prolonged, the forecast

295 skills of 3C-vine model outperformed the MG model for most regions of China (e.g., Figures 5e and  
296 5f, accounting 72% and 74% of land areas in China for  $\Delta R^2 > 0$  under 2–3-month lead times,  
297 respectively). This indicates the 3C-vine model sufficiently utilized the forecasted information  
298 contained by previous meteorological drought and agricultural drought persistence in comparison  
299 with the MG model under the same conditions.

300 The forecast ability of 3C-vine model, compared with the MG model, is limited over climate  
301 region D5 (e.g., Figures 5b and 5c). This may be related to the fact that D5 is a crucial grain-  
302 producing region in China (Lu et al., 2012; Xiao et al., 2019; Zhang et al., 2016), the intensive  
303 anthropogenic activities (e.g., irrigation and urbanization) may alter the linkage between  
304 meteorological drought and agricultural drought, as well as the strength of agricultural drought  
305 memory (AghaKouchak et al., 2021). To ensure food security, if D5 experiences a drought event at  
306 the previous stage, agricultural managers and policymakers would mitigate the drought through  
307 irrigation in a variety of ways, such as groundwater exploitation and reservoir operation (Zhang et  
308 al., 2016). However, under this circumstance, the soil water obtaining the supplement from the  
309 irrigation water would affect the performance of agricultural drought forecast.

310 -----**Figure 5.**-----

311 In contrast with the MG model, the 3C-vine model yielded a better forecast performance for  
312 August under 1–3-month leads agricultural drought across most areas of China, except for the  
313 climate region D5.

#### 314 **4.3. Case study and sub-climate region assessment**

315 The severe drought hit most regions of China in summer 2018, especially in southern and

316 northern China, as the western North Pacific subtropical high abnormally impacted (Liu and Zhu,  
317 2019; Zhang et al., 2020; Zhang et al., 2018). We chose the agricultural drought that occurred in  
318 August of 2018 as a case study to investigate the forecast ability of 3C-vine model. Similarly, the  
319 MG model was selected as a benchmark model. Figure 6 presents the SSI observations and 1–3-  
320 month lead SSI forecasts for this agricultural drought using the 3C-vine model and MG model.  
321 Obviously, the 1–3-month lead SSI forecasts via 3C-vine model resembled the observations (Figures  
322 6a–6d), which captured the droughts that emerged in southern China, northern China, and  
323 northeastern China, i.e., climate regions D1–D2 and D4–D6. Comparing the 3C-vine model with  
324 the MG model under 2–3-month leads (Figures 6c–6d versus Figures 6f–6g), we observed the  
325 deteriorating forecast skill of MG model in climate region D5, which tended to non-drought state  
326 (i.e.,  $SSI > 0$ ), but the 3C-vine model better forecasted the agricultural drought for these regions  
327 under the same conditions, although the severity of agricultural drought had some decrement. The  
328 above analyses indicated that the 3C-vine model, using previous meteorological drought and  
329 agricultural drought persistence as two predictors, had the ability for reliable drought forecast over  
330 many regions of China.

331 -----**Figure 6.**-----

332 -----**Figure 7.**-----

333 Furthermore, to explore the skill of 3C-vine model in capturing the extremum of agricultural  
334 drought (i.e., minimum and maximum SSIs), we randomly selected a typical region (black rectangle  
335 boxes in Figure 6b) in each climate region. Note that these extreme SSI values were calculated using  
336 the spatial average in each typical region. Figures 7a and 7b shows the probability density function  
337 (PDF) curve of minimum and maximum SSIs for these selected typical regions (D1S–D7S) via the



338 3C-vine model and MG model for 1–3-month leads of August. Here, the vertical black dash line  
339 denotes the SSI observation in each subplot. The  $x$ -axis value of peak point (i.e., high probability)  
340 for each PDF curve is regarded as the best estimation of SSI under diverse lead times. With the 3C-  
341 vine model as an example (analogously for the MG model), for minimum SSI with 1–2-month lead  
342 times, the difference between forecasted SSI and observed SSI was slight (except for D3S), which  
343 all reflected the drought state for these typical regions (Figure 7a). The deteriorated skills of 3C-vine  
344 and MG models in a typical region D3S may be attributed to the lengthy response time existing  
345 between precipitation deficiency and soil moisture shortage, which is caused by the limited  
346 precipitation that cannot effectively replenish the soil moisture depletion due to the incrustation of  
347 vadose zone. For the 3-month lead time, the poor forecasts were produced in a typical region D5S  
348 for the minimum SSI. This phenomenon may result in the agricultural manager utilizing irrigation  
349 to mitigate the effect of drought on crop growth, thus, the response relationship between  
350 meteorological drought and agricultural drought accordingly would change (Xu et al., 2021b).

351 For the forecasted maximum SSI utilizing 3C-vine model (analogously for the MG model) over  
352 diverse regions, the excellence forecast ability is displayed for the 1–3-month leads (Figure 7b),  
353 excluding the typical regions D5S and D6S (PDF curve shifted left). For the abundant precipitation  
354 and higher soil moisture content in D6S, the shortened response time between precipitation and soil  
355 moisture (Xu et al., 2021b) may cause inferior forecasts of 3C-vine model for the target month.

356 To display the robustness of 3C-vine model for forecasting agricultural drought in any month  
357 of interest, we further forecasted extreme agricultural drought in July for D1S–D7S (Figures 7c and  
358 7d). The difference between forecasted and observed extreme SSIs for the MG model is larger than  
359 that of 3C-vine model in distinct typical regions, e.g., the forecasted maximum SSI in July on D4S

360 (Figure 7d). The width of PDF curve qualitatively provides an estimation of forecast uncertainty of  
361 3C-vine model and MG model. As shown in Figure 7, in comparison with the 3C-vine model, we  
362 found that the width of PDF curves in the MG model are broadened, indicating that the MG model  
363 produced more pronounced uncertainty for agricultural drought forecast. Furthermore, the skills of  
364 MG model tended to deteriorate over many selected typical regions, especially for 2–3-month lead  
365 times of July and August. Generally, compared with the MG model under different lead times,  
366 agricultural drought forecasts made by the 3C-vine model are more accurate across different typical  
367 regions, in terms of predictive uncertainty (i.e., the width of PDF curve) as well as the difference  
368 between observed and forecasted extreme SSIs (Figures 7).

369 Moreover, to assess the forecast performance (according to  $NSE$ ,  $R^2$ , and  $RMSE$ ) of the 3C-vine  
370 model over each climate region, we counted the pixel contained in each climate region and  
371 constructed the boxplots for these performance metrics (Figures 5j–5l). We still selected the MG  
372 model as the reference model, and obtained the difference between these two models, i.e.,  $\Delta NSE$ ,  
373  $\Delta R^2$ , and  $\Delta RMSE$ . The forecast performances of 3C-vine model and MG model were generally  
374 consistent for 1-month lead of August over climate regions D1–D7 (Figures 5j–5l, the median  
375 percentile of  $\Delta NSE$ ,  $\Delta R^2$ , and  $\Delta RMSE$  were all around the 0 line), indicating the improved skills of  
376 3C-vine model was limited under the same condition. Obviously, the median percentile of  $\Delta NSE$   
377 and  $\Delta R^2$  were greater than 0 as well as  $\Delta RMSE$  was lower than 0, respectively, for 2–3-month leads  
378 SSI forecast of August in different climate regions D1–D7 (except for D5), indicating that the 3C-  
379 vine model shows a better performance than the MG model in forecasting agricultural drought over  
380 diverse climate regions of China.

381 In conclusion, based the ability of typical agricultural drought forecasted (Figure 6) and

382 extremum agricultural drought captured in selected typical regions (Figure 7) and the comprehensive  
383 forecast performance showed in diverse climate regions (Figures 5j–5l), the 3C-vine model had a  
384 good forecast skill for 1–3-month leads agricultural drought of August over most areas of China.

## 385 **5. Discussion and Conclusions**

386 This study developed a C-vine copula model for forecasting agricultural drought over China  
387 under three dimensions, in which antecedent meteorological drought and agricultural drought  
388 persistence were employed as two predictors. We selected the MG model as a competition model,  
389 in terms of the difference in NSE,  $R^2$ , and RMSE between 3C-vine and MG models, to evaluate the  
390 forecast performance of 3C-vine model. These performance metrics all displayed that the 3C-vine  
391 model, especially for 2–3-month lead times, outperformed the MG model in many climate regions  
392 over China (except for D5, which lies in humid and subhumid regions of northern China) (Figure 5).  
393 Compared with the MG model, the 3C-vine model yielded a good forecast skill for the selected  
394 typical agricultural droughts (Figure 5). Besides, the nearly perfect forecast of extremum agricultural  
395 drought in typical regions (Figure 7) further certified the excellent ability of 3C-vine model.

396 Heterogeneous topography and anthropogenic activities (e.g., irrigation and urbanization) have  
397 certainly impacted precipitation interpolation and soil moisture simulation, which may depart from  
398 the actual precipitation or soil moisture conditions, notwithstanding the precipitation of CN05.1 and  
399 soil moisture of ERA5 show good performances with respect to drought monitoring and forecasting  
400 over China (Wang and Yuan, 2021; Wu et al., 2021a; Xu et al., 2009; Zhang et al., 2021; Zhang et  
401 al., 2019). It can also influence the response (propagation) time from meteorological drought to  
402 agricultural drought as well as agricultural drought memory and can thus lead to the 3C-vine model  
403 falling short in some climate regions. To address this issue, we can comprehensively utilize multiple

404 reanalysis data sets, e.g., the precipitation and soil moisture data in Global Land Data Assimilation  
405 System (GLDAS) and ERA5, to reduce the uncertainty resulting from a single data source (Wang  
406 and Yuan, 2021; Wu et al., 2021a). Currently, it is a challenge to consider irrigation activities into  
407 agricultural drought forecasting, especially at large spatial scales. In addition to antecedent  
408 precipitation deficit, air temperature, relative humidity, and evapotranspiration may influence soil  
409 moisture budget. Moreover, from the perspective of driving mechanisms, the effect of certain  
410 atmospheric circulation anomalies (e.g., El Niño-Southern Oscillation (ENSO), Pacific Decadal  
411 Oscillation (PDO), and North Arctic Oscillation (NAO)) on agricultural drought at regional and  
412 global scales can also be considered as predictors (Zhang et al., 2021). Therefore, a more efficient  
413 space can be established by leveraging these predictors for forecasting agricultural drought.

414 In recent years, a myriad of extreme events, such as heatwaves and flash droughts, have swept  
415 many regions around the globe. These extreme events have a rapid onset with a few days or weeks  
416 and lead to devastating impacts on agricultural production, water resource security, and human well-  
417 being (Wang and Yuan, 2021; Yuan et al., 2019; Zscheischler et al., 2020). Therefore, agricultural  
418 drought forecasting at finer temporal scales (e.g., weekly) is essential for agricultural managers and  
419 policymakers to manage and plan water use. Yet, with limited spatiotemporal resolution and the  
420 length of model sample, we temporally have not carried out agricultural drought forecasting at sub-  
421 monthly or pentad temporal scales.

422 The limitation of this study is that we choose a “best” model from two C-vine copula candidate  
423 models (i.e., Figure 2) as the ideal forecast. However, as the inherent structural differences (i.e.,  
424 ordering variables are different), the utilized best model may underestimate the forecast uncertainty  
425 (Liu et al., 2021a). Therefore, to reduce the predictive uncertainty and improve the forecast

426 performance, a multi-model combination technique (e.g., Bayesian model averaging (Liu et al.,  
427 2021a; Long et al., 2017)) can be considered to merge different C-vine copula candidate models.  
428 Moreover, as we only pay attention to the C-vine copulas and several bivariate copula functions, the  
429 other D-vine copulas or regular vine copulas, as well as a multitude of bivariate copula families  
430 (Sadegh et al., 2017) can be investigated to establish the forecast model for agricultural drought in  
431 the next work.

#### 432 **Data availability**

433 The gridded monthly CN05.1 precipitation data with a 0.25° spatial resolution was provided by  
434 the Climate Change Research Center, Chinese Academy of Sciences (available at  
435 <http://ccrc.iap.ac.cn/resource/detail?id=228>) during the period of 1961–2018. The gridded monthly  
436 soil moisture data with three soil depths (0–7 cm, 7–28 cm, and 28–100 cm) from the European  
437 Center for Medium-Range Weather Forecast (ECMWF) ERA5 reanalysis datasets are available at  
438 1961–1978: [https://cds.climate.copernicus.eu/cdsapp#!/dataset/reanalysis-era5-single-levels-](https://cds.climate.copernicus.eu/cdsapp#!/dataset/reanalysis-era5-single-levels-monthly-means-preliminary-back-extension?tab=overview)  
439 [monthly-means-preliminary-back-extension?tab=overview](https://cds.climate.copernicus.eu/cdsapp#!/dataset/reanalysis-era5-single-levels-monthly-means-preliminary-back-extension?tab=overview) and 1979–2018:  
440 [https://cds.climate.copernicus.eu/cdsapp#!/dataset/reanalysis-era5-single-levels-monthly-](https://cds.climate.copernicus.eu/cdsapp#!/dataset/reanalysis-era5-single-levels-monthly-means?tab=overview)  
441 [means?tab=overview](https://cds.climate.copernicus.eu/cdsapp#!/dataset/reanalysis-era5-single-levels-monthly-means?tab=overview).

#### 442 **Author contribution**

443 Haijiang Wu: Conceptualization, Methodology, Software, Visualization, Writing - original draft.  
444 Xiaoling Su: Writing - review & editing, Data curation, Validation, Investigation, Funding  
445 acquisition, Supervision, Formal analysis. Vijay P. Singh: Writing - review & editing, Supervision.  
446 Te Zhang: Formal analysis, Investigation. Jixia Qi: Data curation, Investigation. Shengzhi Huang:  
447 Writing - review & editing, Investigation.

448 **Competing interests**

449 The authors declare that they have no conflict of interest.

450 **Acknowledgements**

451 The authors would like to thank two anonymous reviewers and Editor Carlo De Michele for  
452 their constructive comments and suggestions which contributed to improving the quality of the paper.

453 This study was financially supported by the National Natural Science Foundation of China (Grants  
454 No. 51879222 and 52079111).

455 **References**

456 Aas, K., and Berg, D.: Models for construction of multivariate dependence – a comparison study,  
457 Eur. J. Financ., 15(7-8), 639–659, <https://doi.org/10.1080/13518470802588767>, 2009.

458 Aas, K., Czado, C., Frigessi, A., and Bakken, H.: Pair-copula constructions of multiple dependence.  
459 Insur. Math. Econ., 44(2), 182–198. <https://doi.org/10.1016/j.insmatheco.2007.02.001>, 2009.

460 AghaKouchak, A., Mirchi, A., Madani, K., Di Baldassarre, G., Nazemi, A., Alborzi, A., Anjileli, H.,  
461 Azarderakhsh, M., Chiang, F., Hassanzadeh, E., Huning, L. S., Mallakpour, I., Martinez, A.,  
462 Mazdiyasn, O., Moftakhari, H., Norouzi, H., Sadegh, M., Sadeqi, D., Van Loon, A. F., and  
463 Wanders, N.: Anthropogenic Drought: Definition, Challenges, and Opportunities, Rev.  
464 Geophys., 59(2), e2019RG000683, <https://doi.org/10.1029/2019rg000683>, 2021.

465 Bedford, T., and Cooke, R. M.: Vines—A new graphical model for dependent random variables, Ann.  
466 Stat., 30(4), 1031–1068, <https://doi.org/10.1214/aos/1031689016>, 2002.

467 Benjamini, Y., and Hochberg, Y.: Controlling the false discovery rate: A practical and powerful  
468 approach to multiple testing, J. R. Stat. Soc. Ser. B-Stat. Methodol., 57(1), 289–300,

469 <https://doi.org/10.1111/j.2517-6161.1995.tb02031.x>, 1995.

470 Bevacqua, E.: CDVineCopulaConditional: Sampling from conditional C- and D-vine copulas, R  
471 package, version 0.1.1, <https://CRAN.R-project.org/package=CDVineCopulaConditional>,  
472 2017a.

473 Bevacqua, E., Maraun, D., Hobæk Haff, I., Widmann, M., and Vrac, M.: Multivariate statistical  
474 modelling of compound events via pair-copula constructions: analysis of floods in Ravenna  
475 (Italy), *Hydrol. Earth Syst. Sci.*, 21(6), 2701–2723, [https://doi.org/10.5194/hess-21-2701-](https://doi.org/10.5194/hess-21-2701-2017)  
476 2017, 2017b.

477 Chen, X., Koenker, R., and Xiao, Z.: Copula-based nonlinear quantile autoregression, *Econom. J.*,  
478 12, S50–S67, <https://doi.org/10.1111/j.1368-423X.2008.00274.x>, 2009.

479 De Michele, C., and Salvadori, G.: A Generalized Pareto intensity-duration model of storm rainfall  
480 exploiting 2-Copulas. *J. Geophys. Res.*, 108(D2), 4067, <https://doi.org/10.1029/2002jd002534>,  
481 2003.

482 De Michele, C., Salvadori, G., Vezzoli, R., and Pecora, S.: Multivariate assessment of droughts:  
483 Frequency analysis and dynamic return period, *Water Resour. Res.*, 49, 6985–6994,  
484 <https://doi.org/10.1002/wrcr.20551>, 2013.

485 Dißmann, J., Brechmann, E. C., Czado, C., and Kurowicka, D.: Selecting and estimating regular  
486 vine copulae and application to financial returns, *Comput. Stat. Data Anal.*, 59, 52–69,  
487 <https://doi.org/10.1016/j.csda.2012.08.010>, 2013.

488 FAO: The impact of disasters and crises on agriculture and food security, Food and Agriculture  
489 Organization of the United Nations, Rome, <https://doi.org/10.4060/cb3673en>, 2021.

490 Favre, A.-C., El Adlouni, S., Perreault, L., Thiémondge, N., and Bobée, B.: Multivariate hydrological  
491 frequency analysis using copulas. *Water Resour. Res.*, 40(1), W01101,

492 <https://doi.org/10.1029/2003wr002456>, 2004.

493 Ganguli, P., and Reddy, M. J.: Ensemble prediction of regional droughts using climate inputs and  
494 the SVM-copula approach, *Hydrol. Process.*, 28(19), 4989–5009.  
495 <https://doi.org/10.1002/hyp.9966>, 2014.

496 Genest, C., Rémillard, B., and Beaudoin, D.: Goodness-of-fit tests for copulas: A review and a power  
497 study, *Insur. Math. Econ.*, 44(2), 199–213, <https://doi.org/10.1016/j.insmatheco.2007.10.005>,  
498 2009.

499 Gringorten, I. I.: A plotting rule for extreme probability paper, *J. Geophys. Res.*, 68(3), 813–814,  
500 <https://doi.org/10.1029/JZ068i003p00813>, 1963.

501 Hao, Z., Hao, F., Singh, V. P., Sun, A. Y., and Xia, Y.: Probabilistic prediction of hydrologic drought  
502 using a conditional probability approach based on the meta-Gaussian model, *J. Hydrol.*, 542,  
503 772–780, <https://doi.org/10.1016/j.jhydrol.2016.09.048>, 2016.

504 Hao, Z., Hao, F., Singh, V. P., and Ouyang W.: Quantitative risk assessment of the effects of drought  
505 on extreme temperature in eastern China, *J. Geophys. Res.-Atmos.*, 122, 9050–9059,  
506 <https://doi.org/10.1002/2017JD027030>, 2017.

507 Hao, Z., Hao, F., Singh, V. P., and Zhang, X.: Statistical prediction of the severity of compound dry-  
508 hot events based on El Niño-Southern Oscillation, *J. Hydrol.*, 572, 243–250.  
509 <https://doi.org/10.1016/j.jhydrol.2019.03.001>, 2019a.

510 Hao, Z., Hao, F., Xia, Y., Singh, V. P., and Zhang, X.: A monitoring and prediction system for  
511 compound dry and hot events, *Environ. Res. Lett.*, 14(11), 114034,  
512 <https://doi.org/10.1088/1748-9326/ab4df5>, 2019b.

513 He, L., Hao, X., Li, H., and Han, T.: How Do Extreme Summer Precipitation Events Over Eastern  
514 China Subregions Change? *Geophys. Res. Lett.*, 48, e2020GL091849,



515 <https://doi.org/10.1029/2020GL091849>, 2021.

516 Hemri, S., Lisniak, D., and Klein, B.: Multivariate postprocessing techniques for probabilistic  
517 hydrological forecasting, *Water Resour. Res.*, 51(9), 7436–7451,  
518 <https://doi.org/10.1002/2014wr016473>, 2015.

519 Joe, H.: Families of m-variate distributions with given margins and  $m(m-1)/2$  bivariate dependence  
520 parameters, *Institute of Mathematical Statistics Lecture Notes – Monograph Series*  
521 *Distributions with fixed marginals and related topics*, 120–141,  
522 <https://doi.org/10.1214/lnms/1215452614>, 1996.

523 Joe, H.: *Dependence modeling with copulas*, Chapman and Hall/CRC, 2014.

524 Lesk, C., Rowhani, P., and Ramankutty, N.: Influence of extreme weather disasters on global crop  
525 production, *Nature*, 529(7584), 84–87, <https://doi.org/10.1038/nature16467>, 2016.

526 Liu, B., and Zhu, C.: Extremely Late Onset of the 2018 South China Sea Summer Monsoon  
527 Following a La Niña Event: Effects of Triple SST Anomaly Mode in the North Atlantic and a  
528 Weaker Mongolian Cyclone, *Geophys. Res. Lett.*, 46(5), 2956–2963,  
529 <https://doi.org/10.1029/2018gl081718>, 2019.

530 Liu, Z., Cheng, L., Hao, Z., Li, J., Thorstensen, A., and Gao, H.: A Framework for Exploring Joint  
531 Effects of Conditional Factors on Compound Floods, *Water Resour. Res.*, 54(4), 2681–2696,  
532 <https://doi.org/10.1002/2017wr021662>, 2018.

533 Liu, Z., Cheng, L., Lin, K., and Cai, H.: A hybrid bayesian vine model for water level prediction,  
534 *Environ. Modell. Softw.*, 142, 105075, <https://doi.org/10.1016/j.envsoft.2021.105075>, 2021a.

535 Liu, Z., Xie, Y., Cheng, L., Lin, K., Tu, X., and Chen, X.: Stability of spatial dependence structure  
536 of extreme precipitation and the concurrent risk over a nested basin, *J. Hydrol.*, 602, 126766,  
537 <https://doi.org/10.1016/j.jhydrol.2021.126766>, 2021b.

538 Long, D., Bai, L., Yan, L., Zhang, C., Yang, W., Lei, H., Quan, J., Meng, X., and Shi, C.: Generation  
539 of spatially complete and daily continuous surface soil moisture of high spatial resolution,  
540 Remote Sens. Environ., 233, 111364, <https://doi.org/10.1016/j.rse.2019.111364>, 2019.

541 Long, D., Pan, Y., Zhou, J., Chen, Y., Hou, X., Hong, Y., Scanlon, B. R., and Longuevergne, L.:  
542 Global analysis of spatiotemporal variability in merged total water storage changes using  
543 multiple GRACE products and global hydrological models, Remote Sens. Environ., 192, 198–  
544 216, <https://doi.org/10.1016/j.rse.2017.02.011>, 2017.

545 Lu, Y., Wu, K., Jiang, Y., Guo, Y., and Desneux, N.: Widespread adoption of Bt cotton and insecticide  
546 decrease promotes biocontrol services, Nature, 487(7407), 362–365,  
547 <https://doi.org/10.1038/nature11153>, 2012.

548 Ma, F., Luo, L., Ye, A., and Duan, Q.: Seasonal drought predictability and forecast skill in the semi-  
549 arid endorheic Heihe River basin in northwestern China, Hydrol. Earth Syst. Sci., 22, 5697–  
550 5709, <https://doi.org/10.5194/hess-22-5697-2018>, 2018.

551 Modanesi, S., Massari, C., Camici, S., Brocca, L., and Amarnath, G.: Do Satellite Surface Soil  
552 Moisture Observations Better Retain Information About Crop-Yield Variability in Drought  
553 Conditions? Water Resour. Res., 56(2), e2019WR025855,  
554 <https://doi.org/10.1029/2019wr025855>, 2020.

555 Nagler, T., Schepsmeier, U., Stoeber, J., Brechmann, E. C., Graeler, B., Erhardt, T., Almeida, C.,  
556 Min, A., Czado, C., Hofmann, M., Killiches, M., Joe, H., and Vatter, T.: VineCopula: Statistical  
557 Inference of Vine Copulas, R Package Version 2.4.2, [https://CRAN.R-](https://CRAN.R-project.org/package=VineCopula)  
558 [project.org/package=VineCopula](https://CRAN.R-project.org/package=VineCopula), 2021.

559 Nelsen, R. B.: An Introduction to Copulas, 2nd ed., Springer, N. Y., 2013.

560 Orth, R., and Destouni, G.: Drought reduces blue-water fluxes more strongly than green-water fluxes

561 in Europe, *Nat. Commun.*, 9(1), 3602, <https://doi.org/10.1038/s41467-018-06013-7>, 2018.

562 Röthlisberger, M., and Martius, O.: Quantifying the Local Effect of Northern Hemisphere  
563 Atmospheric Blocks on the Persistence of Summer Hot and Dry Spells, *Geophys. Res. Lett.*,  
564 46(16), 10101–10111, <https://doi.org/10.1029/2019gl083745>, 2019.

565 Sadegh, M., Ragno, E., and AghaKouchak, A.: Multivariate Copula Analysis Toolbox (MvCAT):  
566 Describing dependence and underlying uncertainty using a Bayesian framework, *Water Resour.*  
567 *Res.*, 53(6), 5166–5183, <https://doi.org/10.1002/2016wr020242>, 2017.

568 Salvadori, G., and De Michele, C.: Frequency analysis via copulas: Theoretical aspects and  
569 applications to hydrological events. *Water Resour. Res.*, 40(12), W12511,  
570 <https://doi.org/10.1029/2004wr003133>, 2004.

571 Sarhadi, A., Burn, D. H., Concepción Ausín, M., and Wiper, M. P.: Time-varying nonstationary  
572 multivariate risk analysis using a dynamic Bayesian copula, *Water Resour. Res.*, 52(3), 2327–  
573 2349, <https://doi.org/10.1002/2015wr018525>, 2016.

574 Sklar, A.: *Fonctions de Répartition à Dimensions et Leurs marges*, 8, Publications de l’Institut de  
575 Statistique de L’Université de Paris, Paris, France, 1959.

576 Su, B., Huang, J., Fischer, T., Wang, Y., Kundzewicz, Z. W., Zhai, J., Sun, H., Wang, A., Zeng, X.,  
577 Wang, G., Tao, H., Gemmer, M., Li, X., and Jiang, T.: Drought losses in China might double  
578 between the 1.5 degrees C and 2.0 degrees C warming, *P. Natl. Acad. Sci. USA*, 115(42),  
579 10600–10605, <https://doi.org/10.1073/pnas.1802129115>, 2018.

580 Vernieuwe, H., Vandenberghe, S., De Baets, B., and Verhoest, N. E. C.: A continuous rainfall model  
581 based on vine copulas, *Hydrol. Earth Syst. Sci.*, 19(6), 2685–2699,  
582 <https://doi.org/10.5194/hess-19-2685-2015>, 2015.

583 Wang, W., Dong, Z., Lall, U., Dong, N., and Yang, M.: Monthly Streamflow Simulation for the

584 Headwater Catchment of the Yellow River Basin With a Hybrid Statistical-Dynamical Model,  
585 Water Resour. Res., 55(9), 7606–7621, <https://doi.org/10.1029/2019wr025103>, 2019.

586 Wang, Y., and Yuan, X.: Anthropogenic Speeding Up of South China Flash Droughts as Exemplified  
587 by the 2019 Summer-Autumn Transition Season, Geophys. Res. Lett., 48(9), e2020GL091901,  
588 <https://doi.org/10.1029/2020gl091901>, 2021.

589 Wilks, D. S.: Statistical methods in the atmospheric sciences, Academic Press, 2014.

590 Wilks, D. S.: “The Stippling Shows Statistically Significant Grid Points”: How Research Results are  
591 Routinely Overstated and Overinterpreted, and What to Do about It, B. Am. Meteorol. Soc.,  
592 97(12), 2263–2273, <https://doi.org/10.1175/bams-d-15-00267.1>, 2016.

593 Wu, H., Su, X., Singh, V. P., Feng, K., and Niu, J.: Agricultural Drought Prediction Based on  
594 Conditional Distributions of Vine Copulas, Water Resour. Res., 57(8), e2021WR029562,  
595 <https://doi.org/10.1029/2021wr029562>, 2021a.

596 Wu, H., Su, X., and Zhang, G.: Prediction of agricultural drought in China based on Meta-Gaussian  
597 model, Acta Geogr. Sin., 76(3), 525–538, <https://doi.org/10.11821/dlxb202103003>, 2021b.

598 Wu, J., Chen, X., Yu, Z., Yao, H., Li, W., and Zhang, D.: Assessing the impact of human regulations  
599 on hydrological drought development and recovery based on a ‘simulated-observed’  
600 comparison of the SWAT model. J. Hydrol., 577, 123990,  
601 <https://doi.org/10.1016/j.jhydrol.2019.123990>, 2019.

602 Wu, J., Gao, X., Giorgi, F., and Chen, D.: Changes of effective temperature and cold/hot days in late  
603 decades over China based on a high resolution gridded observation dataset, Int. J. Climatol.,  
604 37, 788–800, <https://doi.org/10.1002/joc.5038>, 2017.

605 Xiao, G., Zhao, Z., Liang, L., Meng, F., Wu, W., and Guo, Y.: Improving nitrogen and water use  
606 efficiency in a wheat-maize rotation system in the North China Plain using optimized farming

607 practices, *Agric. Water Manage.*, 212, 172–180, <https://doi.org/10.1016/j.agwat.2018.09.011>,  
608 2019.

609 Xiong, L., Yu, K.-x., and Gottschalk, L.: Estimation of the distribution of annual runoff from climatic  
610 variables using copulas, *Water Resour. Res.*, 50(9), 7134–7152,  
611 <https://doi.org/10.1002/2013wr015159>, 2014.

612 Xu, L., Chen, N., Chen, Z., Zhang, C., and Yu, H.: Spatiotemporal forecasting in earth system science:  
613 Methods, uncertainties, predictability and future directions. *Earth-Sci. Rev.*, 222, 103828,  
614 <https://doi.org/10.1016/j.earscirev.2021.103828>, 2021a.

615 Xu, Y., Gao, X., Shen, Y., Xu, C., Shi, Y., and Giorgi, F.: A daily temperature dataset over China and  
616 its application in validating a RCM simulation, *Adv. Atmos. Sci.*, 26(4), 763–772,  
617 <https://doi.org/10.1007/s00376-009-9029-z>, 2009.

618 Xu, Y., Zhang, X., Hao, Z., Singh, V. P., and Hao, F.: Characterization of agricultural drought  
619 propagation over China based on bivariate probabilistic quantification, *J. Hydrol.*, 598, 126194,  
620 <https://doi.org/10.1016/j.jhydrol.2021.126194>, 2021b.

621 Yao, N., Li, Y., Lei, T., and Peng, L.: Drought evolution, severity and trends in mainland China over  
622 1961-2013, *Sci. Total Environ.*, 616–617, 73–89,  
623 <https://doi.org/10.1016/j.scitotenv.2017.10.327>, 2018.

624 Yuan, X., Wang, L., Wu, P., Ji, P., Sheffield, J., and Zhang, M.: Anthropogenic shift towards higher  
625 risk of flash drought over China, *Nat. Commun.*, 10(1), 4661, [https://doi.org/10.1038/s41467-](https://doi.org/10.1038/s41467-019-12692-7)  
626 019-12692-7, 2019.

627 Zhang, J., Mu, Q., and Huang, J.: Assessing the remotely sensed Drought Severity Index for  
628 agricultural drought monitoring and impact analysis in North China, *Ecol. Indic.*, 63, 296–309,  
629 <https://doi.org/10.1016/j.ecolind.2015.11.062>, 2016.

630 Zhang, L., and Singh, V. P.: Copulas and their applications in water resources engineering,  
631 Cambridge University Press, 2019.

632 Zhang, L., Zhou, T., Chen, X., Wu, P., Christidis, N., and Lott, F. C.: The late spring drought of 2018  
633 in South China, *Bull. Amer. Meteorol. Soc.*, 101(1), S59–S64, [https://doi.org/10.1175/BAMS-](https://doi.org/10.1175/BAMS-D-19-0202.1)  
634 [D-19-0202.1](https://doi.org/10.1175/BAMS-D-19-0202.1), 2020.

635 Zhang, Q., Qi, T., Singh, V. P., Chen, Y. D., and Xiao, M.: Regional Frequency Analysis of Droughts  
636 in China: A Multivariate Perspective, *Water Resour. Manag.*, 29(6), 1767–1787,  
637 <https://doi.org/10.1007/s11269-014-0910-x>, 2015.

638 Zhang, Q., Li, Q., Singh, V. P., Shi, P., Huang, Q., and Sun, P.: Nonparametric integrated  
639 agrometeorological drought monitoring: Model development and application, *J. Geophys.*  
640 *Res.-Atmos.*, 123, 73–88, <https://doi.org/10.1002/2017JD027448>, 2018.

641 Zhang, Q., Yu, H., Sun, P., Singh, V. P., and Shi, P.: Multisource data based agricultural drought  
642 monitoring and agricultural loss in China, *Glob. Planet. Change*, 172, 298–306,  
643 <https://doi.org/10.1016/j.gloplacha.2018.10.017>, 2019.

644 Zhang, T., Su, X., and Feng, K.: The development of a novel nonstationary meteorological and  
645 hydrological drought index using the climatic and anthropogenic indices as covariates, *Sci.*  
646 *Total Environ.*, 786, 147385, <https://doi.org/10.1016/j.scitotenv.2021.147385>, 2021.

647 Zhang, X., Su, Z., Lv, J., Liu, W., Ma, M., Peng, J., and Leng, G.: A Set of Satellite-Based Near  
648 Real-Time Meteorological Drought Monitoring Data over China, *Remote Sens.*, 11(4), 453,  
649 <https://doi.org/10.3390/rs11040453>, 2019.

650 Zhang, Y., Hao, Z., Feng, S., Zhang, X., Xu, Y., and Hao, F.: Agricultural drought prediction in China  
651 based on drought propagation and large-scale drivers, *Agric. Water Manage.*, 255, 107028,  
652 <https://doi.org/10.1016/j.agwat.2021.107028>, 2021.

653 Zhang, Y., Wang, Z., Sha, S., and Feng, J.: Drought Events and Its Causes in Summer of 2018 in  
654 China. *J. Arid Meteorol.*, 36(5), 884–892, [https://doi.org/10.11755/j.issn.1006-7639\(2018\)-05-](https://doi.org/10.11755/j.issn.1006-7639(2018)-05-0884)  
655 0884, 2018.

656 Zhao, S.: A new scheme for comprehensive physical regionalization in China, *Acta Geogr. Sin.*,  
657 38(1), 1–10, 1983.

658 Zhou, S., Williams, A. P., Berg, A. M., Cook, B. I., Zhang, Y., Hagemann, S., Lorenz, R., Seneviratne,  
659 S. I., and Gentile, P.: Land-atmosphere feedbacks exacerbate concurrent soil drought and  
660 atmospheric aridity, *P. Natl. Acad. Sci. USA*, 116(38), 18848–18853,  
661 <https://doi.org/10.1073/pnas.1904955116>, 2019.

662 Zscheischler, J., Martius, O., Westra, S., Bevacqua, E., Raymond, C., Horton, R. M., van den Hurk,  
663 B., AghaKouchak, A., Jézéquel, A., Mahecha, M. D., Maraun, D., Ramos, A. M., Ridder, N.  
664 N., Thiery, W., and Vignotto, E.: A typology of compound weather and climate events, *Nature*  
665 *Reviews Earth & Environment*, 1(7), 333–347, <https://doi.org/10.1038/s43017-020-0060-z>,  
666 2020.

667

668

## Figure Captions

669 **Figure 1.** Seven sub-climate regions division over China. The specific information of climate  
670 regions D1–D7 is listed at the left-bottom in the panel.

671 **Figure 2.** Different schematic (two types) of C-vine copulas under three-dimensional scenarios. For  
672 the first type (a), the ordering variables are  $y_1$ ,  $y_2$ , and  $y_3$ , while for the second type (b) that  
673 are  $y_2$ ,  $y_1$ , and  $y_3$ .  $C_{12}(C_{21})$ ,  $C_{13}(C_{23})$ , and  $C_{23|1}(C_{13|2})$  denotes bivariate copulas with  
674 parameters  $\theta_{11}$ ,  $\theta_{12}$ , and  $\theta_{21}$ , respectively. Here,  $\theta_{ij}$  signifies the parameters of the  $j$ -th edge  
675 with respect to the  $i$ -th tree.  $G(\bullet|\bullet)$  denote conditional distribution functions.

676 **Figure 3.** Flowchart of agricultural drought forecasting based on canonical vine copulas (3C-vine)  
677 and meta-Gaussian (MG) model under three-dimensional scenarios. Here,  $t$  denotes the  
678 target month (e.g., August);  $i$  signifies the lead times (1–3-months); LOOCV is the  
679 abbreviation of leave-one-out cross validation;  $y_1^{-yr}(y_2^{-yr})$  indicates the series after  
680 removing a sample ( $y_1^{yr}(y_2^{yr})$ ) for a specific year; and  $y_3^{yr}$  is the agricultural drought forecast  
681 value for the target month of a specific year. Note that the optimal tree structure ( $i$  or  $ii$  on  
682 the right-hand side of this figure) is selected based on AIC to forecast agricultural drought.

683 **Figure 4.** Spatial patterns of 1–3-months lag Kendall’s correlation coefficient ( $\tau_k$ ) between  $SPI_{t-i}$  and  
684  $SSI_t$  ( $t$  denotes August, and  $i$  is 1–3-month lag time) (top row), as well as  $SSI_{t-i}$  and  $SSI_t$   
685 (bottom row) for August during 1961–2018 over China. Note the stippling indicates where  
686  $\tau_k$  is at a 0.05 significance level, which is corrected via the false discovery rate (FDR) of  
687 0.1.

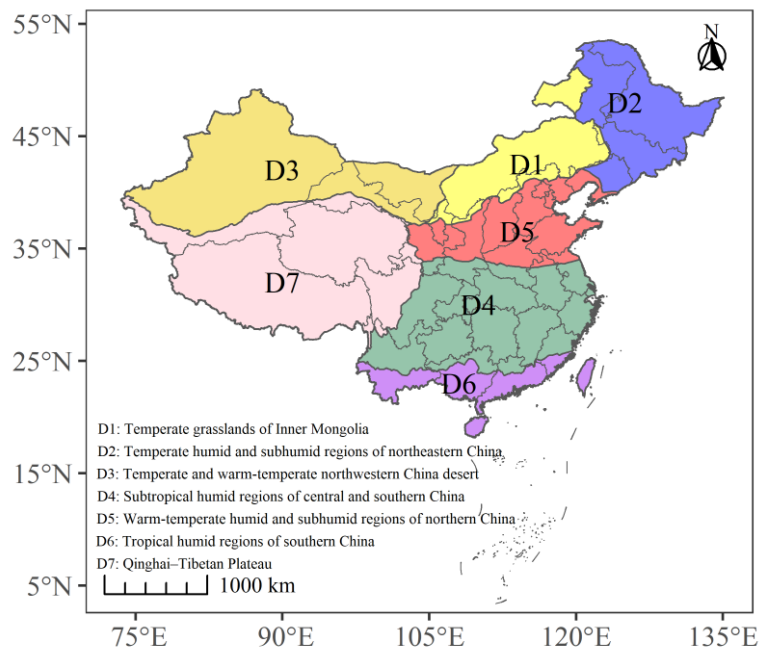
688 **Figure 5.** Forecast performance based on (a–c)  $\Delta NSE$  (difference of  $NSE$  between 3C-vine and MG



689 models,  $NSE_{3C}-NSE_{MG}$ ), (d–f)  $\Delta R^2$  ( $R^2_{3C}-R^2_{MG}$ ), and (g–i)  $\Delta RMSE$  ( $RMSE_{3C}-RMSE_{MG}$ ) for  
 690 the 1–3-month leads of August during 1961–2018 over China. The corresponding boxplots  
 691 of (j)  $\Delta NSE$ , (k)  $\Delta R^2$ , and (l)  $\Delta RMSE$  relative to a threshold of 0 (horizontal black dash line)  
 692 for agricultural drought forecast in August under 1–3-month leads in climate regions D1–  
 693 D7 over China. The percentage of  $\Delta NSE > 0$ ,  $\Delta R^2 > 0$ , and  $\Delta RMSE < 0$  is listed in the left-  
 694 bottom of corresponding sub-figure, respectively.

695 **Figure 6.** SSI observations in August of 2018 (a) as well as the corresponding SSI forecasts under  
 696 1–3-month lead times utilizing 3C-vine model (b–d) and MG model (e–g) over China. The  
 697 black rectangle boxes (as shown in b) denote the typical regions (corresponding to signify  
 698 D1S–D7S) selected in climate regions D1–D7.

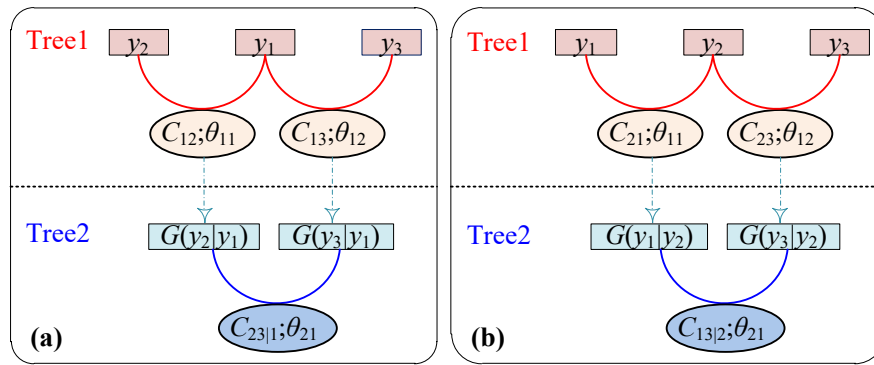
699 **Figure 7.** Probability density function (PDF) curve of (a and c) minimum and (b and d) maximum  
 700 SSI under 1–3-month lead times for August and July during the 1961–2018 period over  
 701 seven selected typical regions in climate regions D1–D7 (i.e., these black rectangle boxes  
 702 in Figure 6b correspond to signify D1S–D7S, respectively). Black dash line and text  
 703 indicate the minimum and maximum observations of SSI in August and July over D1S–  
 704 D7S. These texts with red (green), blue (yellow), and cyan (coral) colors of left (right) in  
 705 each sub-figure are SSI forecasts under 1–3-month lead times of August or July via 3C-  
 706 vine model (MG model), which correspond to the abscissa projected by the peak point of  
 707 each PDF.



708

709 **Figure 1.** Seven sub-climate regions division over China. The specific information of climate

710 regions D1–D7 is listed at the left-bottom in the panel.



711

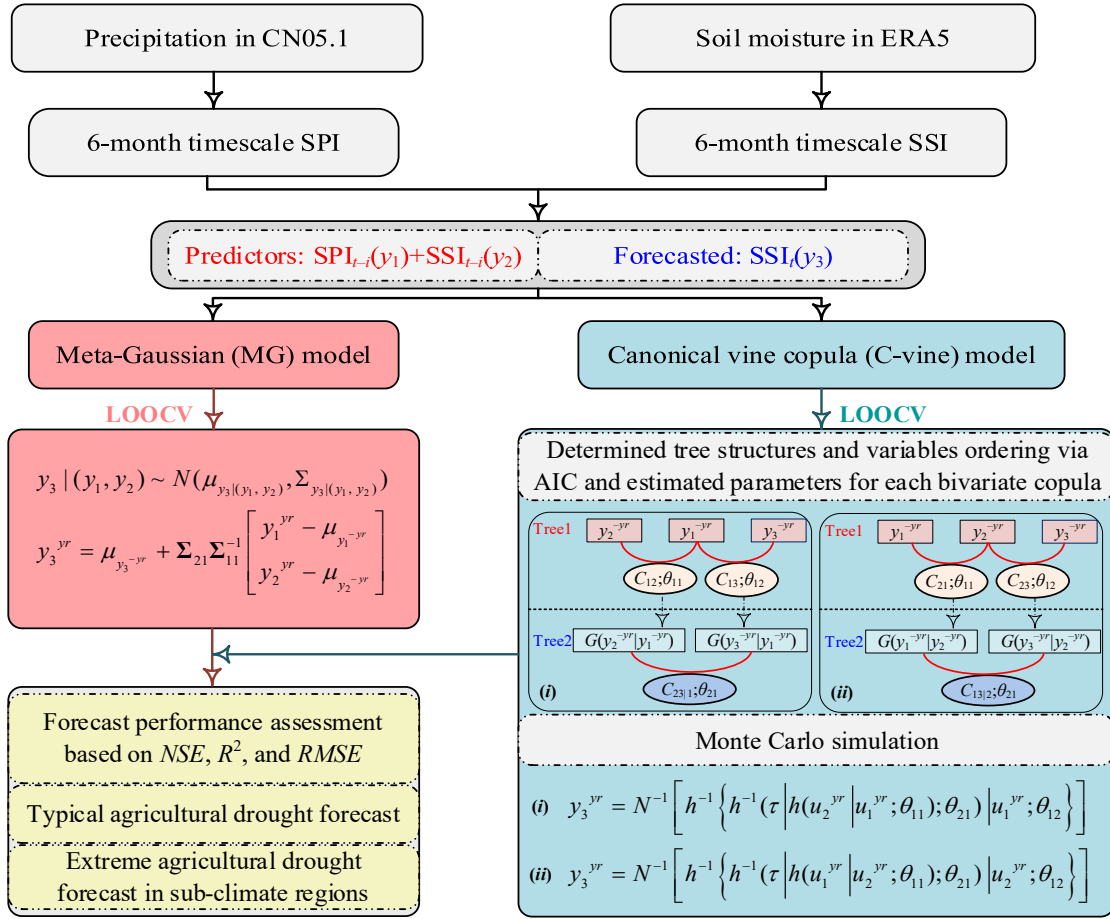
712 **Figure 2.** Different schematic (two types) of C-vine copulas under three-dimensional scenarios. For

713 the first type (a), the ordering variables are  $y_1, y_2,$  and  $y_3,$  while for the second type (b) that are  $y_2, y_1,$

714 and  $y_3.$   $C_{12}(C_{21}), C_{13}(C_{23}),$  and  $C_{23|1}(C_{13|2})$  denotes bivariate copulas with parameters  $\theta_{11}, \theta_{12},$  and  $\theta_{21},$

715 respectively. Here,  $\theta_{ij}$  signifies the parameters of the  $j$ -th edge with respect to the  $i$ -th tree.  $G(\bullet|\bullet)$

716 denote conditional distribution functions.



717

718 **Figure 3.** Flowchart of agricultural drought forecasting based on canonical vine copulas (3C-vine)

719 and meta-Gaussian (MG) model under three-dimensional scenarios. Here,  $t$  denotes the target month

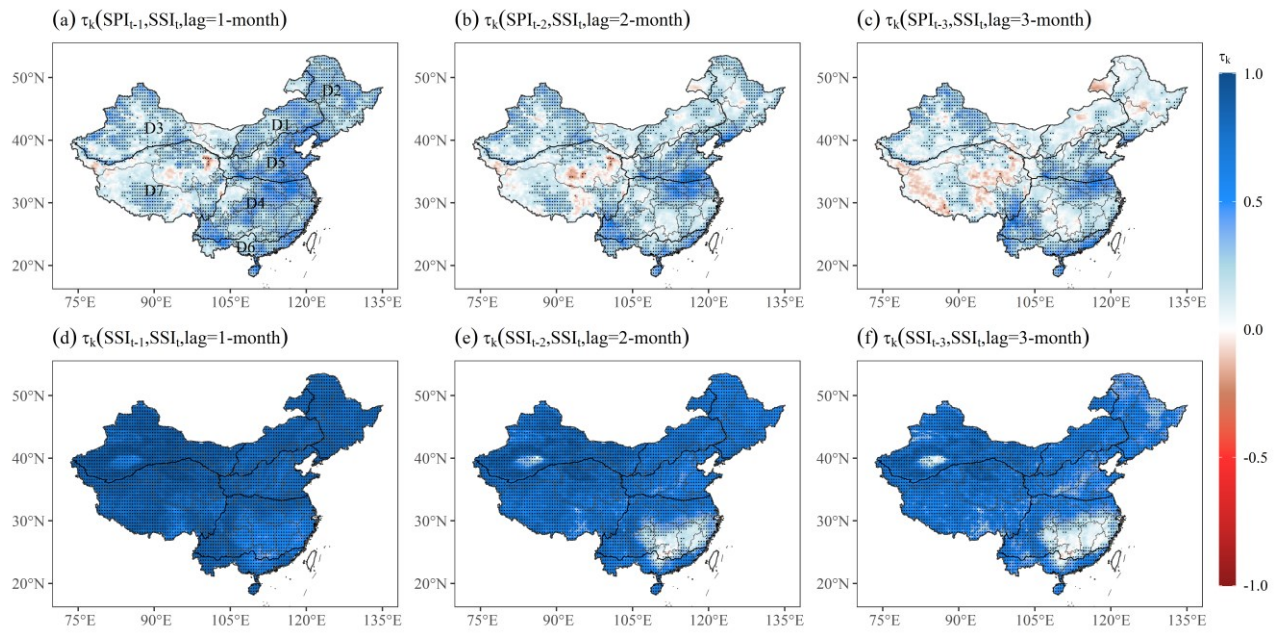
720 (e.g., August);  $i$  signifies the lead times (1–3-months)); LOOCV is the abbreviation of leave-one-

721 out cross validation;  $y_1^{-yr}(y_2^{-yr})$  indicates the series after removing a sample ( $y_1^{yr}(y_2^{yr})$ ) for a specific

722 year; and  $y_3^{yr}$  is the agricultural drought forecast value for the target month of a specific year. Note

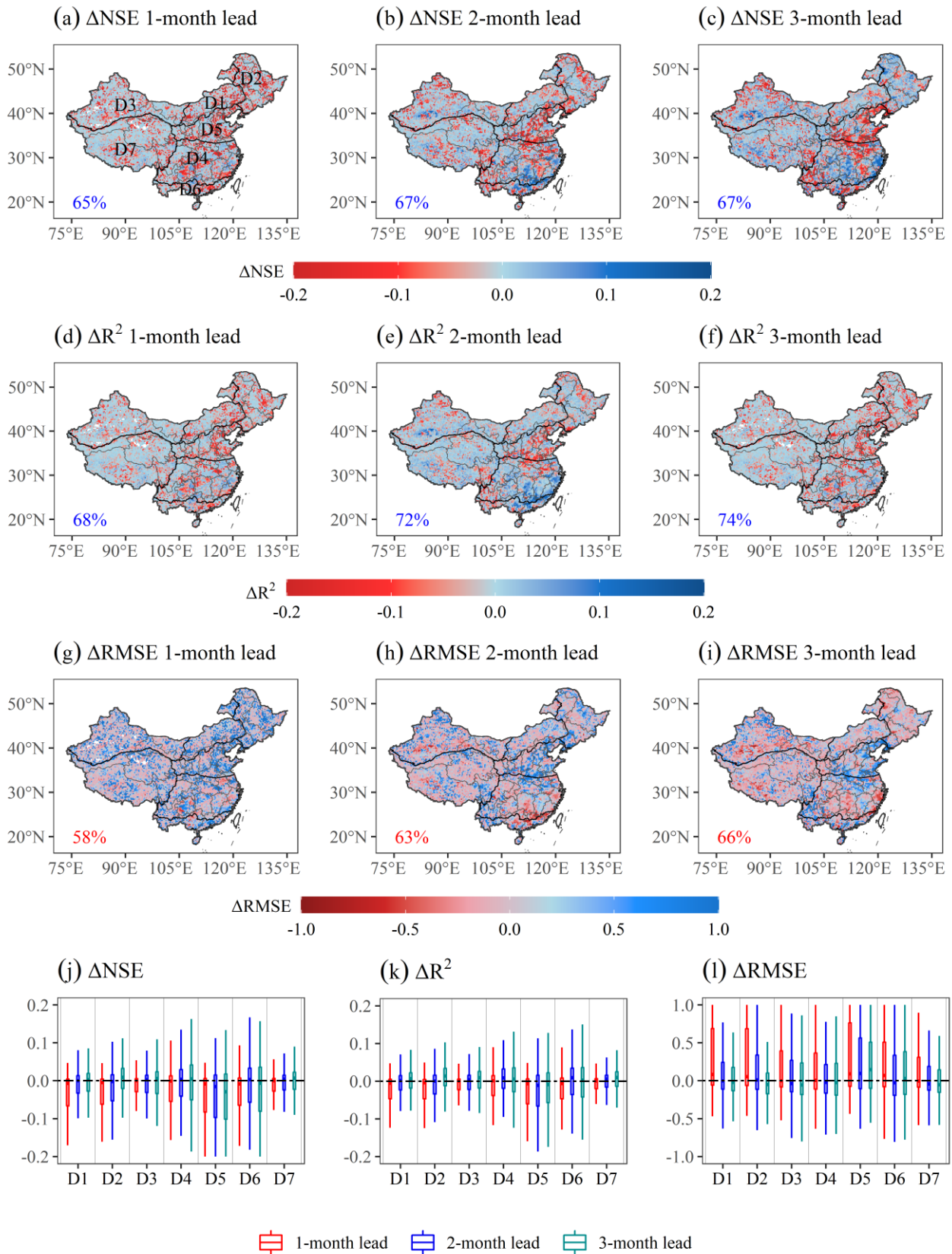
723 that the optimal tree structure ( $i$  or  $ii$  on the right-hand side of this figure) is selected based on AIC

724 to forecast agricultural drought.



725

726 **Figure 4.** Spatial patterns of 1–3-months lag Kendall’s correlation coefficient ( $\tau_k$ ) between SPI $_{t-i}$  and  
 727 SSI $_t$  ( $t$  denotes August, and  $i$  is 1–3-month lag time) (top row), as well as SSI $_{t-i}$  and SSI $_t$  (bottom  
 728 row) for August during 1961–2018 over China. Note the stippling indicates where  $\tau_k$  is at a 0.05  
 729 significance level, which is corrected via the false discovery rate (FDR) of 0.1.

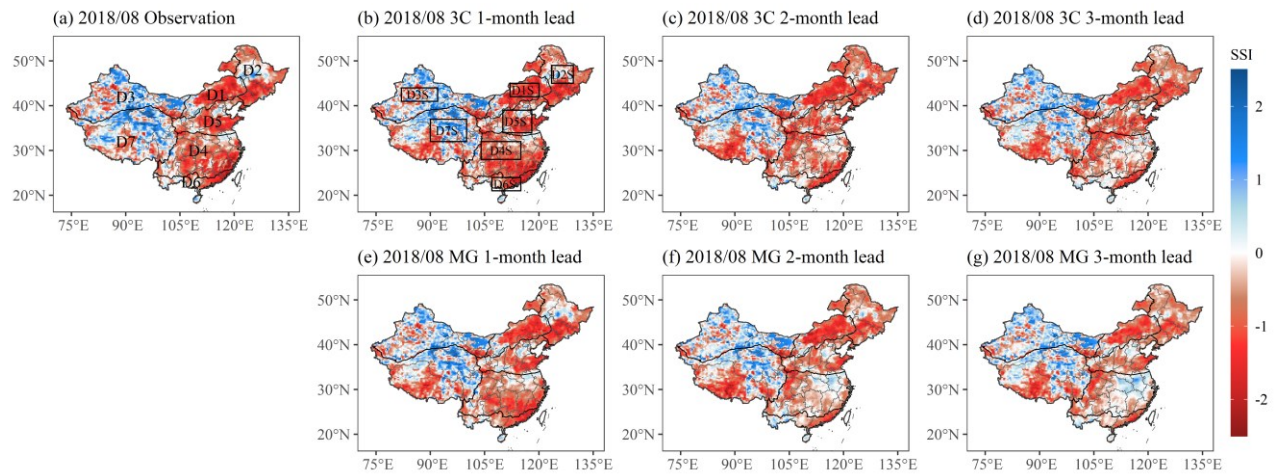


730

731 **Figure 5.** Forecast performance based on (a–c)  $\Delta NSE$  (difference of  $NSE$  between 3C-vine and

732 MG models,  $NSE_{3C} - NSE_{MG}$ ), (d–f)  $\Delta R^2$  ( $R^2_{3C} - R^2_{MG}$ ), and (g–i)  $\Delta RMSE$  ( $RMSE_{3C} - RMSE_{MG}$ ) for the

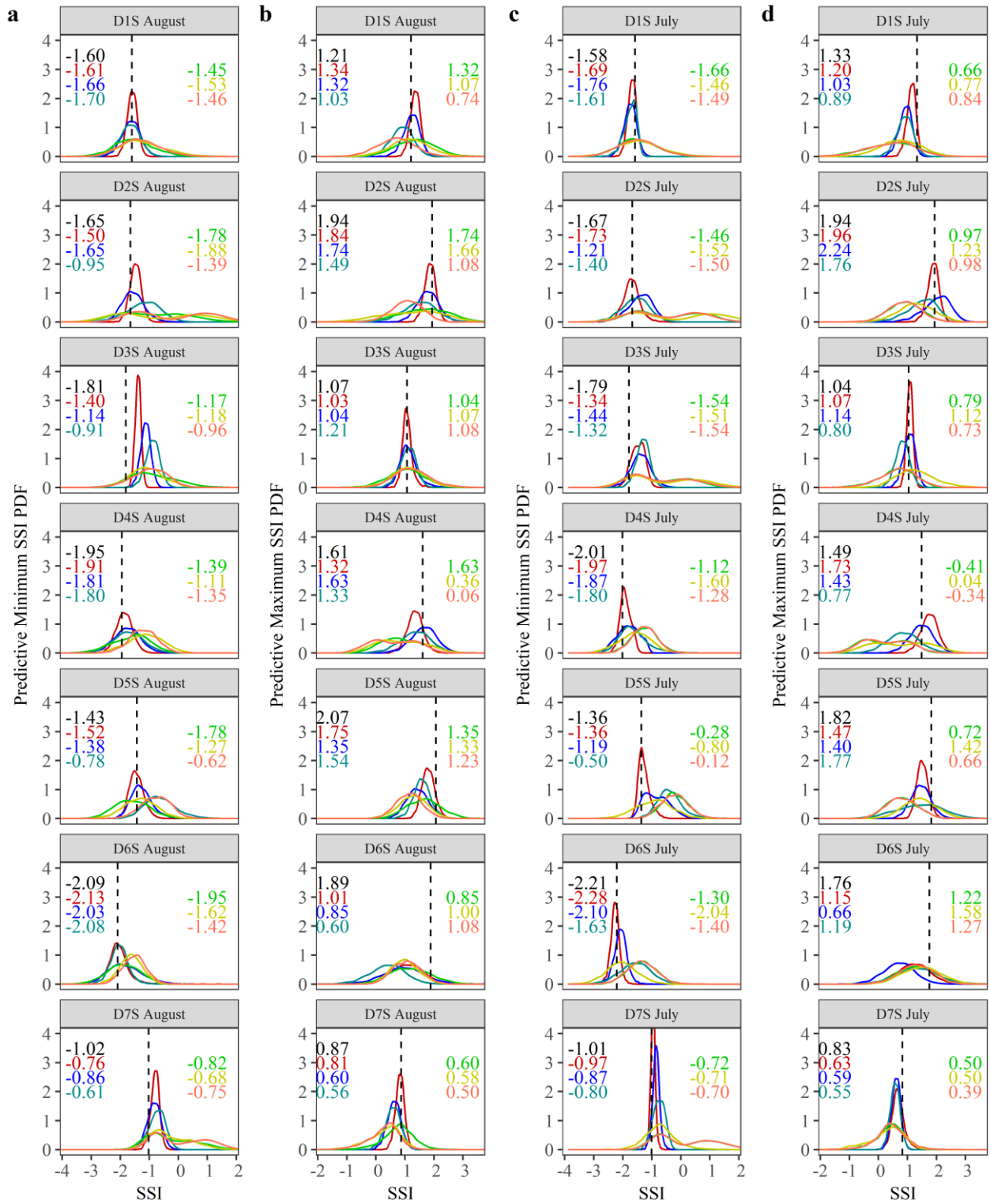
733 1–3-month leads of August during 1961–2018 over China. The corresponding boxplots of (j)  $\Delta NSE$ ,  
734 (k)  $\Delta R^2$ , and (l)  $\Delta RMSE$  relative to a threshold of 0 (horizontal black dash line) for agricultural  
735 drought forecast in August under 1–3-month leads in climate regions D1–D7 over China. The  
736 percentage of  $\Delta NSE > 0$ ,  $\Delta R^2 > 0$ , and  $\Delta RMSE < 0$  is listed in the left-bottom of corresponding sub-  
737 figure, respectively.



738

739 **Figure 6.** SSI observations in August of 2018 (a) as well as the corresponding SSI forecasts under  
 740 1–3-month lead times utilizing 3C-vine model (b–d) and MG model (e–g) over China. The black  
 741 rectangle boxes (as shown in b) denote the typical regions (corresponding to signify D1S–D7S)  
 742 selected in climate regions D1–D7.





743 — 3C 1-month lead — 3C 2-month lead — 3C 3-month lead — MG 1-month lead — MG 2-month lead — MG 3-month lead

744 **Figure 7.** Probability density function (PDF) curve of (a and c) minimum and (b and d) maximum  
 745 SSI under 1–3-month lead times for August and July during the 1961–2018 period over seven  
 746 selected typical regions in climate regions D1–D7 (i.e., these black rectangle boxes in Figure 6b

747 correspond to signify D1S–D7S, respectively). Black dash line and text indicate the minimum and  
748 maximum observations of SSI in August and July over D1S–D7S. These texts with red (green), blue  
749 (yellow), and cyan (coral) colors of left (right) in each sub-figure are SSI forecasts under 1–3-month  
750 lead times of August or July via 3C-vine model (MG model), which correspond to the abscissa  
751 projected by the peak point of each PDF.